Embedded-atom potential for $B2$-NiAl

Y. Mishin

School of Computational Sciences, George Mason University, Fairfax, Virginia 22030

M. J. Mehl and D. A. Papaconstantopoulos

Center for Computational Materials Science, Naval Research Laboratory, Washington, DC 20375-5345

An embedded-atom potential has been constructed for the intermetallic compound $B2$-NiAl by fitting to both experimental properties and *ab initio* data. The *ab initio* data have been generated in the form of energy-volume relations for a number of alternative structures of NiAl and Ni_3Al, as well as for Ni and Al. The potential accurately reproduces the basic lattice properties of $B2$-NiAl, planar faults, and point-defect characteristics. It also reproduces the energetics and stability of all other structures included in the fit. The potential is applied to calculate equilibrium point-defect concentrations in $B2$-NiAl as functions of temperature and composition near the stoichiometry. In contrast to previous calculations, the defect formation entropies arising from atomic vibrations are included in our calculation within the quasiharmonic approximation. Such entropies tend to increase the concentrations of thermal point defects in $B2$-NiAl at high temperatures, but the atomic disorder mechanism remains triple-defect type up to the melting point.

I. INTRODUCTION

The importance of intermetallic compounds of the Ni-Al system for high-temperature structural applications[1] has motivated the strong interest in their fundamental properties. Such properties include interatomic bonding, long-range order and disorder, crystalline defects, and the role of defects in the mechanical behavior, diffusion, and other processes. Some of these properties have recently been studied by first-principles (*ab initio*) calculations.[2–22] Because *ab initio* methods are computationally expensive, the calculations have been limited to relatively small supercells with around 50 atoms and implemented a simple atomic relaxation by minimizing the total energy of the supercell (molecular statics). Although *ab initio* calculations provide significant insights into atomic bonding and some basic properties of lattice defects in nickel aluminides, many other properties and phenomena of interest can only be modeled correctly by using much larger simulation blocks and more sophisticated computer simulation methods such as molecular dynamics, harmonic lattice dynamics, Monte Carlo, and others. Large simulation blocks are accessed by parameter-based semi-empirical methods, such as the many-body potentials of the embedded-atom method[23] (EAM) and Finnis-Sinclair[24] (FS) potentials. For the $B2$-ordered compound NiAl (CsCl prototype), which is the main subject of this paper, EAM and FS potentials have recently been applied to the simulations of dislocations,[25–27] grain boundaries,[28–30] fracture cracks,[31,32] and point defects.[33–38] There is a demand for increasingly more accurate and transferable potentials that could further enhance the reliability of atomistic simulations.

It is the purpose of this paper to present an EAM potential for $B2$-NiAl that is fit to accurately reproduce the lattice properties and defects in this compound, with emphasis on point defects and atomic disorder. We generate the potential using the methodology applied in the previous work.[28,33,39–45] Namely, the potential parametrizes a fitting database that includes both experimental properties of $B2$-NiAl and a large set of structural energies generated by *ab initio* calculations. Additional *ab initio* data, not included in the fitting database, are used to test the potential. The fitting database samples a large area of configuration space in order to enhance the transferability of the obtained potential. The potential proposed in this work can be used effectively in atomistic simulations of plastic deformation, fracture, and especially atomic disorder and diffusion. It is designed to be particularly reliable in high-temperature simulations of $B2$-NiAl using molecular dynamics and Monte Carlo methods.

Previous EAM-type potentials for the Ni-Al system have been reviewed by Baskes.[46] Two more recent potentials have been proposed in Refs. 34 (EAM potential) and 28 (FS potential). All potentials reproduce the lattice parameter, cohesive energy, and elastic constants of $B2$-NiAl fairly well. There are two properties, however, that most potentials fail to reproduce satisfactorily. First, the antiphase boundary (APB) energy on the (110) plane must be 0.5 J/m^2 or higher according to experimental observations.[47] *Ab initio* calculations[3,6] are in agreement with this estimate. Most potentials, however, give lower APB energies: for example, 0.32 J/m^2 (Ref. 48) or 0.29 J/m^2 (Ref. 49). The potential of Ludwig and Gumbsch[33] gives the highest APB energy (0.82 J/m^2), followed by the values of 0.45 J/m^2 (Ref. 28) and 0.43 J/m^2 (Ref. 50), which can also be viewed as acceptable. The APB energy determines the preferred slip system in the compound and is important in simulations of plastic deformation and fracture.

Second, $B2$-NiAl is considered to be a triple-defect compound, at least at low pressures.[19,51] Namely, derivations from the exact stoichiometry toward Al-rich compositions are predominantly accommodated by vacancies on the Ni sublattice, whereas Ni-rich compositions are dominated by antistructural Ni atoms (Ni antisites) on the Al sublattice.[52] This mechanism of atomic disorder was verified experimen-

tally by room-temperature measurements of the lattice parameter as a function of composition.[53,54] More recent high-temperature x-ray measurements indicate significantly lower concentrations of Ni vacancies and higher concentrations of Al antisites in comparison with predictions of the triple-defect model.[55] This was interpreted as evidence against the existance of structural vacancies,[56,57] but the latter conclusion was criticized based on experimental problems and/or an incorrect interpretation of the experimental data.[58] Overall, the existence of structural vacancies in Al-rich NiAl can be viewed as an established experimental fact.

In terms of point-defect energies, the predominance of Ni structural vacancies in Al-rich compositions is due to their energy being lower in comparison with Al antisites on the Ni sublattice. The relevant energy difference, called the interbranch-Al energy,[19] must be positive and sufficiently high to secure the predominance of structural vacancies. The interbranch-Al energy at zero temperature has been evaluated by *ab initio* calculations to give 0.32 (Ref. 7), 0.88 (Ref. 18), 1.28 (Ref. 19), and 1.07 (Ref. 21) eV. Despite the significant scatter of these values, they all confirm the triple-defect mechanism, in agreement with the mentioned experimental data. In contrast, semiempirical potentials give negative values of the interbranch-Al energy with only three exceptions. The EAM potential of Ref. 34 predicts 0.49 eV for this energy, which is a very reasonable number, but the potential underestimates the APB energy (0.33 J/m^2) and disagrees significantly with *ab initio* energies of alternative structures of NiAl. The EAM potential of Ludwig and Gumbsch[33] and the FS potential of Yan *et al.*[28] both give about 0.07 eV for the interbranch-Al energy. Both potentials demonstrate very good agreement with other properties of $B2$-NiAl, but this low value of the interbranch-Al energy essentially makes the disorder mechanism transient between the triple-defect and antisite types.

The proposed EAM potential addresses these two problems by giving 0.55 J/m^2 for the APB energy and 0.48 eV for the interbranch-Al energy, while keeping the agreement with all other properties of $B2$-NiAl at the same high level as the potentials of Ludwig and Gumbsch[33] and Yan *et al.*[28] We will be using the potential of Ludwig and Gumbsch for comparison with our potential throughout the paper. It will be referred to as the LG potential.

II. POTENTIAL GENERATION

A. Fitting database

For $B2$-NiAl, the experimental part of the fitting database includes the equilibrium lattice parameter a_0 (Ref. 59), the cohesive energy E_0 (Ref. 60), the elastic constants c_{ij} (Ref. 61), and linear thermal expansion factors at several temperatures (Ref. 62). For the $L1_2$-ordered compound Ni$_3$Al and pure Ni and Al, only the lattice parameters and cohesive energies are included.[59,60,63,64]

The *ab initio* part of the database includes energy-volume relations for the following structures of NiAl: $B2$, $B1$ (NaCl prototype), $L1_0$ (CuAu prototype), $L1_1$ (CuPt prototype), $B32$ (NaTl prototype), and "40" (NbP prototype).[65] The $L1_0$, $L1_1$, and "40" structures represent alternating Ni and

Al layers parallel to (100), (111), and (210) planes, respectively. Energy-volume relations for the $L1_2$, $D0_{22}$, and $D0_3$ structures[65] with the stoichiometry of Ni$_3$Al are also included in the database, along with those for fcc Ni and Al. Furthermore, in order to represent the APB on the (110) plane in $B2$-NiAl, three "artificial" structures have been designed, which represent the $B2$ structure containing an array of parallel APB's separated by four, six, and eight (110) planes, respectively. The corresponding structures are referred to as APB4, APB6, and APB8, respectively. They are included in the fitting database instead of trying to match a specific value of the APB energy. The energies of all structures mentioned above have been calculated for a set of 10–20 volumes around the equilibrium volume. Because the reference energies involved in *ab initio* and EAM calculations are different, only energy differences between structures can be compared. To facilitate the comparison, all *ab initio* energies relating to the same stoichiometry are shifted by the same amount so that to match the EAM-calculated equilibrium energy of the respective ground-state structure ($B2$-NiAl or $L1_2$-Ni$_3$Al). This shift does not introduce any new approximations and does not have any effect on the fitting procedure. It only allows us to conveniently plot *ab initio* and EAM energies together.

The *ab initio* structural energies have been calculated using the general-potential linearized augmented plane-wave (LAPW) method.[66,67] The electronic exchange and correlation are specified by the Perdew-Wang parametrization[68] of the local density approximation (LDA) within the Kohn-Sham formulation of the density functional theory.[69] Brillouin zone integrations are performed using the "special" **k**-point set of Monkhorst and Pack,[70] modified[71] to correctly sample the Brillouin zone of lower-symmetry lattices. To speed convergence, we follow Gillan[72] and smear out the electronic eigenvalues with a Fermi distribution at $T = 2$ mRy. We have checked the convergence of both the basis set and **k**-point meshes. Our choice for the plane-wave cutoff of the basis set is $K_{max} = 10.5/R_{mt}$,[73,74] where R_{mt} is the radius of the muffin tins (1.95 bohr in these calculations). For cubic structures, we construct a regular **k**-point mesh with $N_k = 16$ divisions[75] between the Γ point and the zone boundary at X (H in the bcc lattice). For near-equilibrium fcc Ni, these choices lead to secular equations with approximately 200 basis functions and 408 **k** points in the irreducible part of the Brillouin zone. By comparing with smaller values of $R_{mt}K_{max}$ and N_k we estimate that our total energies are converged to better than 0.5 mRy/atom. The calculations for Al, NiAl, and Ni$_3$Al are carried out in a spin-restricted mode, allowing no magnetic moment. Calculations for pure Ni are carried out using the spin-polarized LDA by artificially inducing a magnetic moment on the Ni ions in the starting charge density and iterating to self-consistency. LDA calculations are known to slightly underestimate lattice periods of crystals. To partly compensate for this effect, all LDA data used for generating the EAM potential are modified by multiplying all interatomic distances by the ratio of the experimental and LDA-predicted lattice periods of $B2$-NiAl. The LAPW method is also used for calculating the energy along the tetragonal and trigonal deformation paths in

$B2$-NiAl. These energies are not included in the fitting database but are used for testing the potential.

Finally, in order to secure the triple-defect mechanism of disorder, the interbranch-Al energy[19] in $B2$-NiAl is required to lie within the range of values 0.8 ± 0.4 eV, which approximately represents the *ab initio* data available in the literature.[7,18,19,21,51]

B. Parametrization and fitting procedures

In the EAM model,[23] the total energy of a binary system A-B is represented as

$$E_{\text{tot}} = \frac{1}{2} \sum_{ij} \Phi_{\alpha_i - \alpha_j}(r_{ij}) + \sum_i F_{\alpha_i}(\bar{\rho}_i). \tag{1}$$

Here $\Phi_{\alpha_i - \alpha_j}(r_{ij})$ is a pair interaction potential as a function of distance r_{ij} between atoms i and j that have chemical sorts α_i and α_j ($=A$ or B), and F_{α_i} is the embedding energy of an atom of chemical sort α_i as a function of the host electron density $\bar{\rho}_i$ induced at site i by all other atoms in the system. The latter is given by

$$\bar{\rho}_i = \sum_{j \neq i} \rho_{\alpha_j}(r_{ij}), \tag{2}$$

where $\rho_{\alpha_j}(r)$ is the electron density function assigned to an atom of chemical sort α_j. This model involves seven potential functions that can be conveniently divided into three groups: (i) $\Phi_{A-A}(r)$, $\rho_A(r)$, and $F_A(\bar{\rho})$ describe atomic interactions in a pure-A system, (ii) $\Phi_{B-B}(r)$, $\rho_B(r)$, and $F_B(\bar{\rho})$ describe atomic interactions in a pure-B system, and (iii) $\Phi_{A-B}(r)$ describes pair interactions between unlike atoms A and B.

An important property of Eq. (1) is the invariance of the total energy under the transformations[76,77]

$$\rho_A(r) \rightarrow s_A \rho_A(r), \tag{3}$$

$$\rho_B(r) \rightarrow s_B \rho_B(r), \tag{4}$$

$$F_A(\bar{\rho}) \rightarrow F_A(\bar{\rho}/s_A), \tag{5}$$

$$F_B(\bar{\rho}) \rightarrow F_B(\bar{\rho}/s_B), \tag{6}$$

$$F_A(\bar{\rho}) \rightarrow F_A(\bar{\rho}) + g_A \bar{\rho}, \tag{7}$$

$$F_B(\bar{\rho}) \rightarrow F_B(\bar{\rho}) + g_B \bar{\rho}, \tag{8}$$

$$\Phi_{A-A}(r) \rightarrow \Phi_{A-A}(r) - 2g_A \rho_A(r), \tag{9}$$

$$\Phi_{B-B}(r) \rightarrow \Phi_{B-B}(r) - 2g_B \rho_B(r), \tag{10}$$

$$\Phi_{A-B}(r) \rightarrow \Phi_{A-B}(r) - g_A \rho_B(r) - g_B \rho_A(r), \tag{11}$$

where s_A, s_B, g_A, and g_B are arbitrary constants. Although these transformations do not affect the total energy, they do change the shape of the potential functions, which makes them an efficient tool in fitting the potential. For any compound of an A-B system, the potential can be reduced to the

so-called effective pair format[76] by choosing $g_A = -F_A'(\bar{\rho}_A^0)$ and $g_B = -F_B'(\bar{\rho}_B^0)$, where $\bar{\rho}_A^0$ and $\bar{\rho}_B^0$ are equilibrium electron densities on atoms in the compound. In this format, the embedding functions $F_A(\bar{\rho})$ and $F_B(\bar{\rho})$ attain extrema (usually, minima) (Ref. 78) at $\bar{\rho}_A^0$ and $\bar{\rho}_B^0$, respectively, which simplifies analytical expressions for lattice constants, dynamical matrix, and other properties. The effective pair format is often used as a base for comparing different potentials for the same system.

There can be two different strategies for generating a potential for a binary system. One is to employ good-quality pure-A and pure-B potentials constructed separately and only fit the cross potential $\Phi_{A-B}(r)$.[77] For example, the LG potential[33] was generated by this scheme using the Ni and Al potentials constructed earlier by Voter and Chen.[79] While very convenient for handling potential databases, this scheme offers only a limited number of parameters that can be used for fitting to the properties of intermediate compounds. The other strategy is to optimize all seven potential functions simultaneously by fitting them to the whole set of data available for the system.[80] This strategy provides more flexibility for selecting one compound and fitting its properties most accurately in comparison with other phases of the system. The weak side is that the quality of pure-A and pure-B potentials produced by this fit may not be as good as when they are constructed separately. Also, this scheme leads to a multiplicity of potential functions for the same phase, depending on whether such functions were fit specifically for this phase or obtained as support functions for other phases.

Both strategies were tried in this work. Attempts were made to optimize only the cross potential $\Phi_{\text{Ni-Al}}(r)$ for $B2$-NiAl by using, as input, either the Voter-Chen potentials for Ni and Al or more recent potentials constructed with *ab initio* input.[44,81] None of these attempts resulted in a satisfactory fit to all target properties of $B2$-NiAl. For example, the potential could be fit to the LAPW structural energies and could give a reasonable value of the (110) APB energy, but the interbranch-Al energy could never be raised above 0.1 eV. This inability to fit all desired properties probably originates from the simplified nature of the EAM, in particular the presence of the directional bonding between atoms which is not included in the model. We therefore had to choose the second strategy, which gave us more fitting parameters and allowed us to meet the target values of $B2$-NiAl properties. Because the focus has been tightened on this compound, the properties of other phases of the Ni-Al system are reproduced less accurately, although are still reasonable. This potential is, therefore, intended for atomistic simulations of $B2$-NiAl and may not work accurately for other phases.

The following parametrization has been found to work best for the potential functions. The pair interaction functions are parametrized as

$$\Phi(r) = [DM(r, r_0, \alpha, q) + \delta] \psi\left(\frac{r - r_c}{h}\right), \tag{12}$$

where

$$M(r, r_0, \alpha, q) = \exp[-q\alpha(r - r_0)] - q\exp[-\alpha(r - r_0)] \tag{13}$$

is a generalized Morse function, and $\psi(x)$ is a cutoff function defined as $\psi(x) = 0$ if $x \geq 0$ and $\psi(x) = x^4/(1 + x^4)$ if $x < 0$. Expression (12) contains seven fitting parameters D, r_0, α, q, δ, r_c, and h. The electron density functions are parametrized as

$$\rho(r) = s[r^2 \exp(-\beta r) + \varepsilon] \psi\left(\frac{r - r_c}{h}\right), \tag{14}$$

with five fitting parameters s, β, ε, r_c, and h. Finally, the embedding energies are represented by cubic polynomials

$$F(\bar{\rho}) = a_1\bar{\rho} + a_2\bar{\rho}^2 + a_3\bar{\rho}^3, \tag{15}$$

with three fitting coefficients a_1, a_2, and a_3. Note that the cutoff function $\psi(x)$ guarantees that the functions $\Phi(r)$ and $\rho(r)$ and their derivatives up to the second one turn smoothly to zero at the cutoff distance r_c. In the present work, a constraint is imposed that the cutoff parameters r_c and h be the same for all functions (12) and (14). The transformation factor s_{Ni} is fixed by the normalizing condition $\bar{\rho}_{Ni}^0 = 1$ (unit

TABLE I. Optimized values of fitting parameters of potential functions for $B2$-NiAl. See Eqs. (12)–(15) in the text for notation. Note that s_{Ni} is fixed, so that there are a total of 30 adjustable parameters.

| Parameter	Value	Parameter	Value
Ni-Ni		Ni-Al	
D (eV)	2.796 75	D (eV)	7.631 81
r_0 (Å)	2.076 75	r_0 (Å)	1.909 09
α (1/Å)	1.696 48	α (1/Å)	1.150 94
q	1.830 66	q	2.592 81
δ (eV)	$-0.275\,37 \times 10^{-1}$	δ (eV)	$-0.460\,36 \times 10^{-1}$
s	0.945 77		
β (1/Å)	1.819 40	Cutoff	
ε	$-0.665\,23 \times 10^{-3}$	R_c (eV)	5.954 14
a_1 (eV)	$0.321\,92 \times 10^2$	h (eV)	0.500 20
a_2 (eV)	3.714 22		
a_3 (eV)	$-2.037\,96$	Transformations	
		g_{Ni} (eV)	$-0.528\,61 \times 10^2$
		g_{Al} (eV)	$-0.189\,07 \times 10^3$
Al-Al			
D (eV)	2.223 12		
r_0 (Å)	3.219 24		
α (1/Å)	3.613 38		
q	1.008 81		
δ (eV)	$0.426\,35 \times 10^{-1}$		
s	0.398 483 9		
β	1.452 22		
ε	$0.949\,20 \times 10^{-2}$		
a_1 (eV)	$0.861\,05 \times 10^2$		
a_2 (eV)	6.276 07		
a_3	$-2.098\,15$		
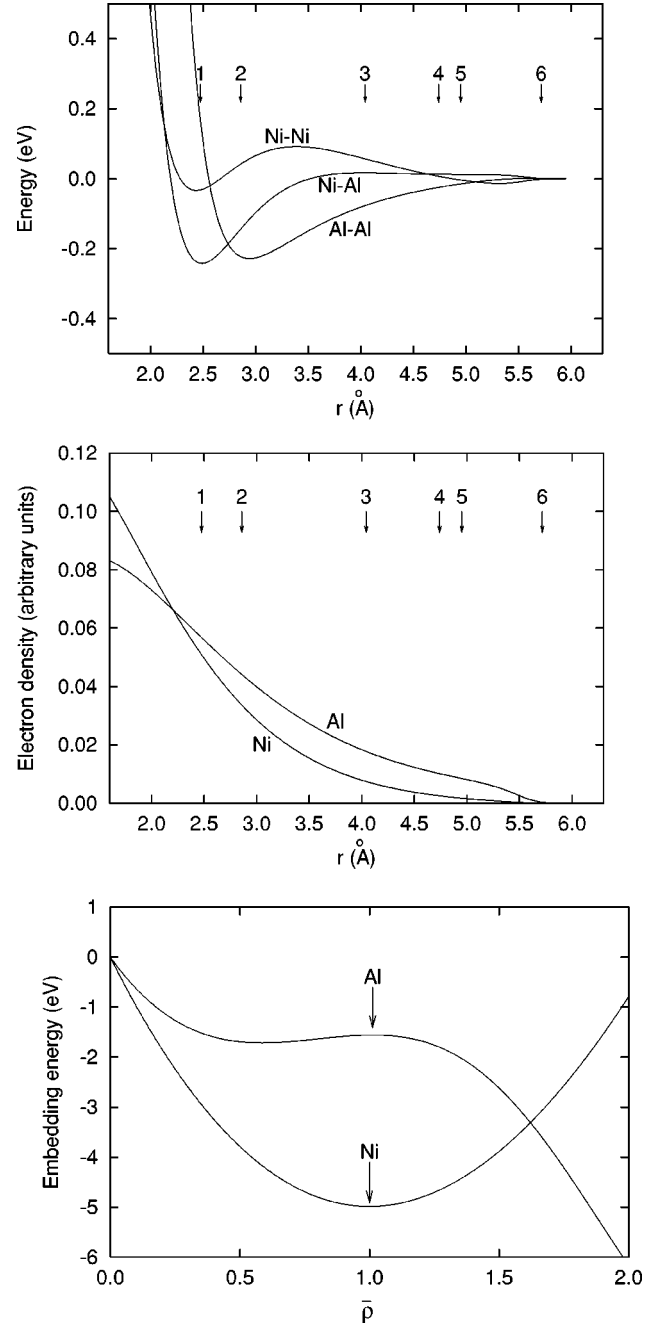
FIG. 1. Potential functions for $B2$-NiAl in the effective pair format: (a) pair interaction functions, (b) electron density functions, and (c) embedding functions. The arrows indicate coordination radii (a), (b) or electron densities on Ni and Al atoms (c) in the equilibrium $B2$-NiAl structure.

electron density on Ni atoms in $B2$-NiAl), while the transformation factors s_{Al}, g_{Ni}, and g_{Al} [see Eqs. (3)–(11)] are used as adjustable parameters. Overall, this parametrization includes 30 fitting parameters.

The potential functions are optimized by minimizing the weighted mean-squared deviation of the properties discussed in Sec. II A from their target values. The weights assigned to different properties serve to represent their relative importance for our purposes.

TABLE II. Experimental lattice properties of *B*2-NiAl fitted by the present EAM potential and LG potential (Ref. 33) in comparison with experimental data.

	Experiment	EAM	LG
a_0 (Å)	2.88[a]	2.86	2.86
E_0 (eV/atom)	−4.50[b]	−4.47	−4.44
c_{11} (10^{11} Pa)	1.99[c]	2.00	1.95
c_{12} (10^{11} Pa)	1.37[c]	1.40	1.41
c_{44} (10^{11} Pa)	1.16[c]	1.20	1.16

[a]Reference 59.
[b]Reference 60.
[c]Reference 61.

C. Fitting results

The obtained fitting parameters are listed in Table I. Figure 1 presents the optimized potential functions plotted in the effective pair format. They are available to the reader, in tabulated form, via the World Wide Web.[82] The cutoff radius of the pair-interaction and electron-density functions is 5.954 Å. The atomic interaction range formally includes six coordination shells of *B*2-NiAl, but the contribution of the sixth shell is almost negligible. The equilibrium electronic densities on atoms are $\bar{\rho}_{Ni}^0 = 1$ and $\bar{\rho}_{Al}^0 = 1.0124$.

III. TESTS AND APPLICATIONS OF THE POTENTIAL

A. Lattice properties

Table II demonstrates that the potential is fit accurately to the experimental values of the lattice parameter, cohesive energy, and elastic constants of *B*2-NiAl. Zone boundary phonon frequencies predicted by the potential are in a fair agreement with experimental data[83] and with the LG potential (Table III). Both potentials tend to overestimate optical frequencies. Note that phonon frequencies were not fitted by the potentials.

TABLE III. Phonon frequencies (in THz) in *B*2-NiAl calculated with the present EAM potential and LG potential (Ref. 33) in comparison with experimental data. Phonon frequencies were not included in the potential fits.

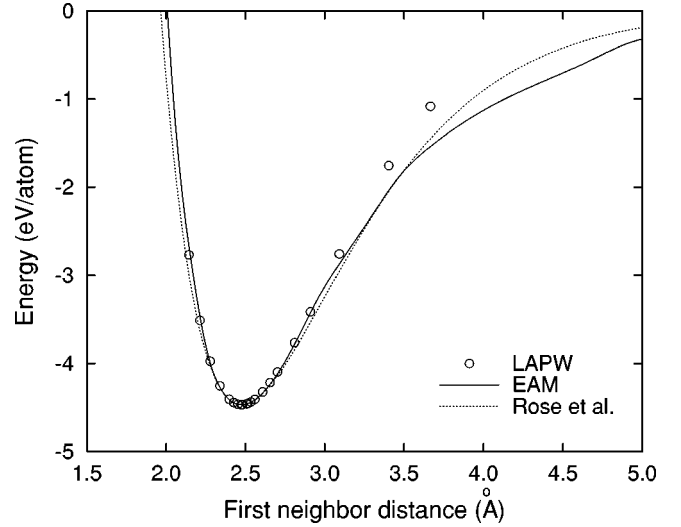| Point	Branch	Experiment[a]	EAM	LG
$\Gamma = [000]$	LO	8.60	10.67	10.45
$X = \frac{1}{2}[001]$	LA	6.05	6.08	5.75
	TA	4.78	5.43	5.93
	LO	10.10	12.23	11.48
	TO	7.72	8.61	8.62
$M = \frac{1}{2}[011]$	LA	4.00	3.30	2.94
	TA	5.60	6.10	5.91
	LO	10.50	13.11	12.15
	TO	7.82	8.30	8.65
$R = \frac{1}{2}[111]$	LA	4.96	5.82	6.16
	LO	9.80	12.25	10.49

[a]Reference 83.

FIG. 2. Comparison of LAPW (○) and EAM-calculated (solid line) equations of state of *B*2-NiAl. All LAPW energies are shifted by the same amount to match the EAM-calculated cohesive energy. The empirical equation of state by Rose *et al.* (Ref. 84) (dotted line) is shown for comparison.

The binding curve calculated with the present potential (Fig. 2) is in good agreement with both LAPW energies and the empirical equation of state by Rose *et al.*,[84] except under very large expansions. The potential also compares favorably with the experimental high-pressure equation of state[85] (Fig. 3), whereas the LG potential tends to overestimate pressures already above 5 GPA. The high-pressure behavior was not included in the fitting database.

Thermal expansion of *B*2-NiAl has been evaluated in two ways: (i) by minimizing the free energy of the lattice with respect to volume expansions in the quasiharmonic approximation[86] using the general quantum-mechanical expression for the vibrational free energy and (ii) by Metropolis Monte Carlo (MC) simulations implemented under zero-pressure conditions (Fig. 4). In both cases, a $6\times6\times6$ block
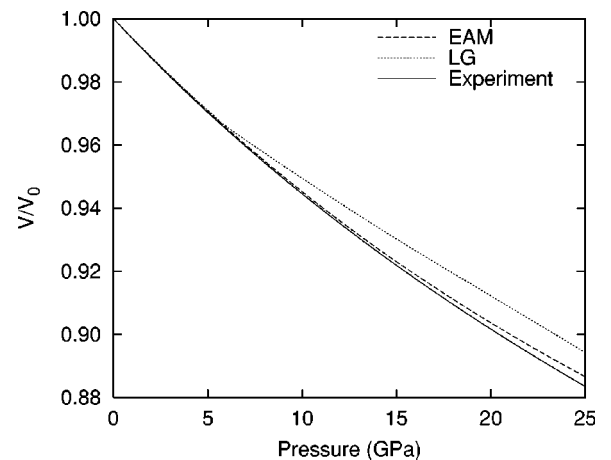

FIG. 3. Pressure-volume relation for NiAl at $T=0$ calculated with the present EAM potential (dashed line) and LG potential (Ref. 33) (dotted line) in comparison with experimental data (Ref. 85). The volume V is normalized by the equilibrium volume V_0.
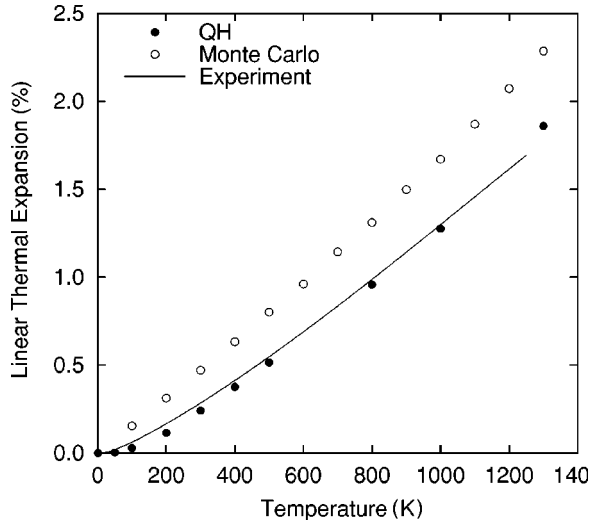
FIG. 4. Linear thermal expansion of $B2$-NiAl calculated in the quasiharmonic approximation (QHA) and by the Monte Carlo method using the present EAM potential. Experimental data (Ref. 62) are shown for comparison.
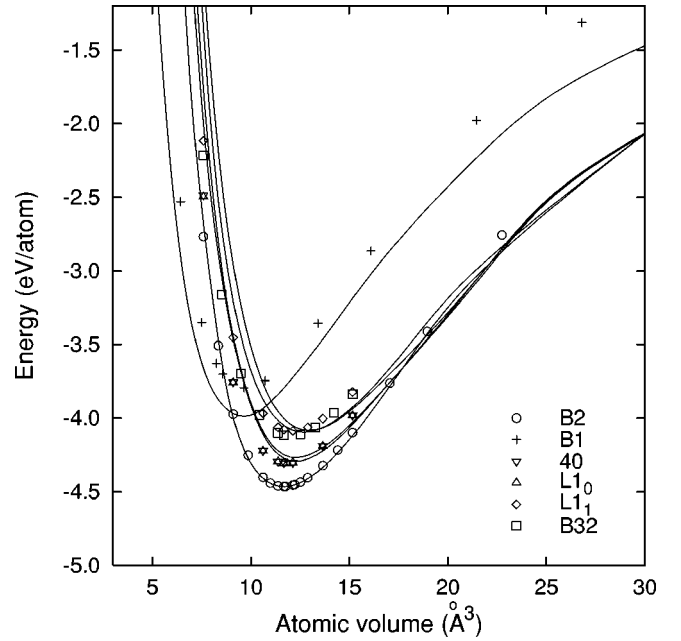

FIG. 5. Comparison of LAPW (symbols) and EAM-calculated (curves) equations of state of different structures of NiAl. Note that LAPW energies of the "40" ($\triangledown$) and $L1_0$ ($\triangle$) structures almost coincide to produce starlike symbols. All LAPW energies are shifted by the same amount to match the EAM-calculated cohesive energy of the $B2$ structure.

with 432 atoms has been used. The Monte Carlo method is more accurate at high temperatures because it includes the unharmonicity of atomic vibrations. The MC-calculated thermal expansion factors lie on the higher side of the experimental data,[62] but the agreement with experiment is reasonable. The quasiharmonic data are more accurate at low temperatures where the quantum effects are important. The quasiharmonic thermal expansion calculated with our potential is in excellent agreement with the experiment (Fig. 4). Calculations with the LG potential give similar results, although the quasiharmonic thermal expansion overestimates the experimental values at high temperatures. The relevant plot is not shown here, but instead Table IV compares the thermal expansion factors calculated at 500 and 1000 K.

B. Structural stability and deformation paths

Figure 5 compares the energy-volume relations (equations of state) of different structures of NiAl obtained by LAPW calculations and with the present potential. Very good agreement is observed between both calculation methods over a relatively wide range of volumes. The potential slightly overbinds the least stable structure $B1$. Very good agreement is also observed for the three Ni$_3$Al structures included in the fitting database (Fig. 6). The $B2$ and $L1_2$ structures are cor-

rectly predicted to be the lowest-energy structures of NiAl and Ni$_3$Al, respectively. To put these results into perspective, Fig. 7 shows the EAM-calculated cohesive energies of different structures, relative to $B2$ and $L1_2$, plotted against the relevant LAPW values. This plot demonstrates again that the relative stability of the structures is accurately and correctly represented by the potential. The long-wavelength mechanical stability of the structures has been tested by calculating the elastic constants. The $L1_0$-NiAl, $B32$-NiAl, and $D0_3$-Ni$_3$Al compounds are found to be unstable against tetragonal distortions ($c_{11} < c_{12}$), while $B1$-NiAl is unstable against trigonal distortions ($c_{44} < 0$). Figure 8 shows that the equations of state of Ni and Al are also in reasonable agreement with LAPW energies and experimental data. Table V summarizes the cohesive energies and lattice parameters of several phases of the Ni-Al system calculated with this potential in comparison with experimental data (when available). For some of the phases, several alternative structures are included in order to demonstrate that the potential cor-

TABLE IV. Linear thermal expansion (in %) of $B2$-NiAl at 500 and 1000 K calculated with the present EAM potential and LG potential (Ref. 33) in comparison with experimental data. QHA: quasiharmonic approximation. MC: Monte Carlo simulations.

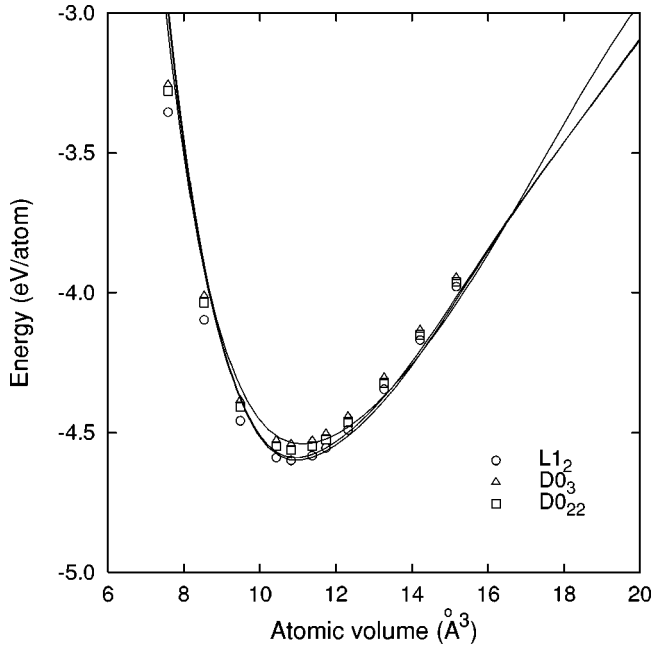| T (K)	Experiment[a]	EAM		LG	
		QHA	MC	QHA	MC
500	0.54	0.52	0.80	0.54	0.75
1000	1.30	1.28	1.67	1.49	1.60

[a]Reference 62.

FIG. 6. Comparison of LAPW (symbols) and EAM-calculated (curves) equations of state of three different structures of Ni_3Al. All LAPW energies are shifted by the same amount to match the EAM-calculated cohesive energy of the $L1_2$ structure.

FIG. 8. Comparison of LAPW (symbols) and EAM-calculated (curves) equations of state of Ni and Al. All LAPW energies relating to the same metal are shifted by the same amount to match the respective experimental cohesive energy.

rectly predicts their energies to be higher than the ground state. For NiAl, the $B20$ structure (FeSi prototype) turns out to be the closest in energy to the ground state, in agreement with previous *ab initio* calculations.[11]

It should be noted that all LAPW energies appearing in Figs. 5–8, as well as the experimental cohesive energies and lattice parameters for $B2$-NiAl, $L1_2$-Ni_3Al, fcc-Ni, and fcc-Al, have been used for fitting the potential. As an indepen-

dent test of the transferability of the potential, the energy along two uniform deformation paths has been calculated and the results are compared with LAPW calculations in Figs. 9 and 10. The first path is the volume conserving Bain path[87] in which the initial $B2$ lattice is stretched along the [100] direction and simultaneously compressed in the [010] and [001] directions. When the c/a ratio of this tetragonal lattice becomes $c/a=\sqrt{2}$, we arrive at an ideal $L1_0$ structure. The fact that the energy does not show any local minimum at $c/a=\sqrt{2}$ (Fig. 9) is consistent with the elastic instability of the $L1_0$ structure mentioned above. The other path is obtained by a trigonal deformation of the $B2$ lattice by stretching it in the [111] direction under a constant volume. The degree of deformation can be measured by the angle θ between the lattice translation vectors, which is initially $\theta = 90°$. At $\theta = 60°$ the structure becomes $B1$ and at $\theta = 33.56°$ it becomes $L1_1$. Again, the fact that the energy of the $B1$ structure is a maximum at $\theta = 60°$ (Fig. 10) is consistent with elastic instability of this structure with $c_{44} < 0$. For both deformation paths, the agreement with LAPW energies is generally good, as it is also for the LG potential. Paidar *et al.*[17] have recently tested the FS potential of Yan *et al.*[28] for the same tetragonal and trigonal deformation paths. The agreement between their *ab initio* energies and the potential predictions is at about the same level as in Figs. 9 and 10. Paidar *et al.* conclude from this comparison that the approximation of central-force many-body potentials is very satisfactory for NiAl. Our calculations lead to the same conclusion.
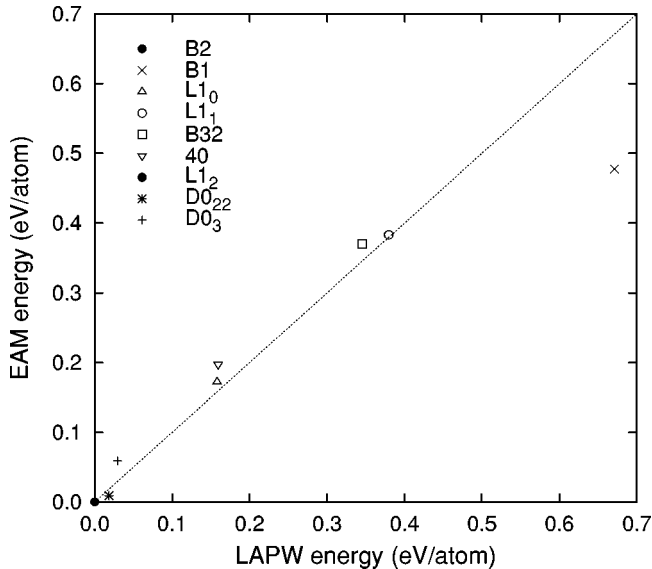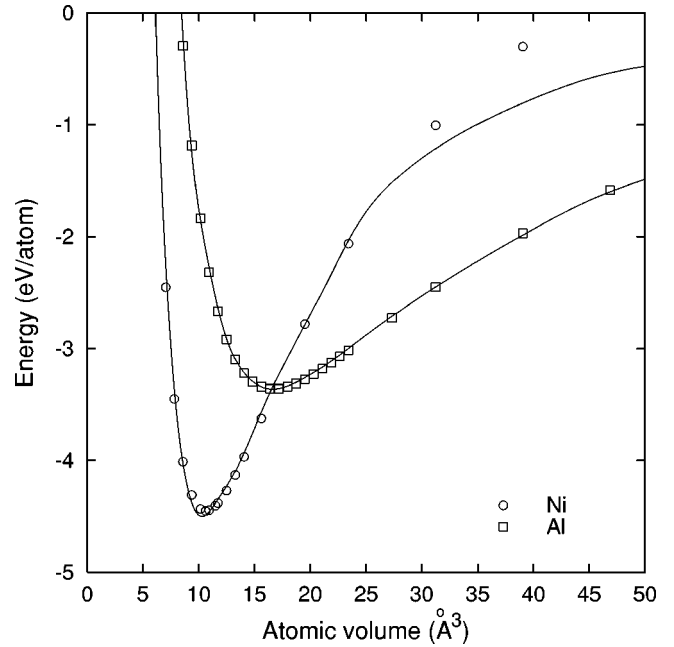

FIG. 7. Comparison of LAPW and EAM-calculated cohesive energies of different structures of NiAl and Ni_3Al relative to the respective ground-state structures ($B2$ and $L1_2$). The line of perfect agreement (dotted line) is shown as a guide to the eye.

C. Planar defects

For surface energies of $B2$-NiAl, no experimental data are available, while results of *ab initio* calculations vary over

TABLE V. Equilibrium lattice parameters (a_0) and cohesive energies (E_0) of selected phases of the Ni-Al system calculated with the present EAM potential. For noncubic structures, two or three lattice parameters are listed separated by commas. Experimental data are included where available. See Ref. 65 for a detailed description of the structures. The asterisk indicates structures which were not included in the potential fit.

Phase	Structure	Experiment		EAM	
		a_0 (Å)	E_0 (eV)	a_0 (Å)	E_0 (eV)
Ni	$A1$	3.52[a]	−4.45[b]	3.453	−4.501
Ni$_3$Al	$L1_2$	3.57[c]	−4.57[d]	3.525	−4.600
	$D0_{22}$			3.523	−4.591
	$D0_3$			2.812	−4.541
	$D0_{11}^*$			4.486, 6.082, 7.144	−4.170
NiAl	$B2$	2.88[a]	−4.50[d]	2.859	−4.465
	$B1$			3.501	−3.988
	$L1_0$			3.662	−4.293
	$L1_1$			3.727	−4.082
	$B32$			2.939	−4.095
	"40"			3.661	−4.268
	$B20^*$			4.600	−4.335
Ni$_3$Al$_4$	Ni$_3$Ga$_4$ type*	11.408[e]		11.375	−4.283
Ni$_2$Al$_3$	$D5_{13}^*$	4.03, 4.88[f]	−4.38[f]	4.016, 4.924	−4.189
NiAl$_3$	$D0_{11}^*$	4.80, 6.60, 7.35[f]	−4.02[f]	4.950, 6.415, 7.484	−3.914
	$L1_2^*$			3.829	−3.805
	$D0_3^*$			3.047	−3.707
	$D0_{22}^*$			3.838	−3.798
Al	$A1$	4.05[a]	−3.36[b]	4.052	−3.362

[a]Reference 59.
[b]Reference 64.
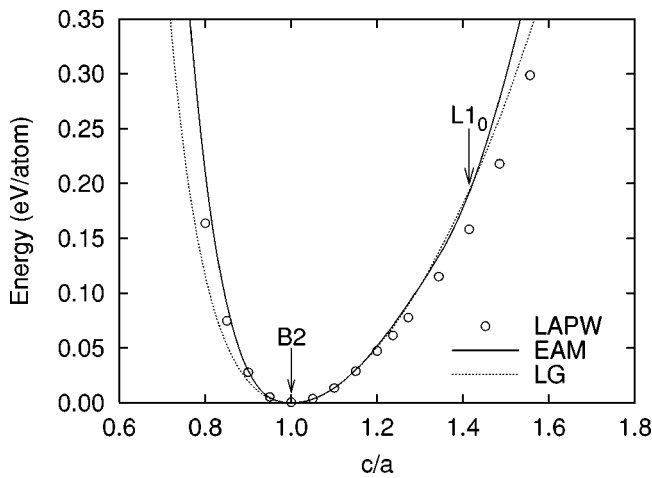[c]Reference 63.
[d]Reference 60.
[e]Reference 96.
[f]Reference 97.

FIG. 9. Energy as a function of the c/a ratio along the Bain path calculated by the LAPW method (○), with the present EAM potential (solid line), and with the LG potential (Ref. 33) (dotted line). Calculations are performed at a constant volume corresponding to the equilibrium $B2$-NiAl structure, and all energies are plotted relative to that structure.
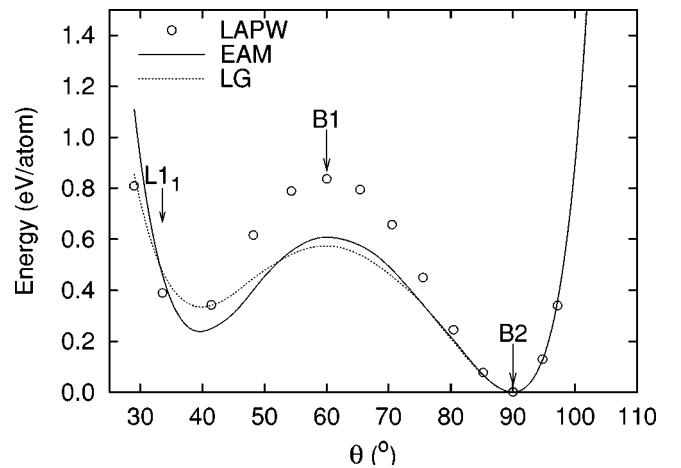

FIG. 10. Energy as a function of the rhombohedral angle θ along the trigonal deformation path calculated by the LAPW method (○), with the present EAM potential (solid line), and with the LG potential (Ref. 33) (dotted line). Calculations are performed at a constant volume corresponding to the equilibrium $B2$-NiAl structure, and all energies are plotted relative to that structure.

TABLE VI. Surface and antiphase boundary (APB) energies (in J/m^2) in $B2$-NiAl calculated with the present EAM potential and LG potential (Ref. 33) in comparison with experimental data and *ab initio* calculations. The asterisk indicates the energy calculated in the generalized gradient approximation.

	Experiment	*Ab initio*	EAM	LG
Surface				
(100)		2.85,[a] 2.75[b]	1.67	1.76
(110)		2.05,[b] 1.87[c]	1.25	1.37
		1.79,[d] 1.37[d*]		
(111)			1.63	1.69
APB				
(110)	>0.50[e]	0.88,[f] 0.81[g]	0.55	0.82
(211)	>0.75[e]	0.89,[f] 0.99[g]	0.72	1.06

[a]Reference 13.   [e]Reference 47.
[b]Reference 4.   [f]Reference 3.
[c]Reference 10.   [g]Reference 6.
[d]Reference 20.

a wide range (Table VI). For the (110) surface that has been studied most extensively, the most recent *ab initio* calculations[20] give 1.79 J/m^2 in the LDA approximation and 1.37 J/m^2 in the generalized gradient approximation. The latter number is considered to be an underestimate.[20] For the (100) and (111) surfaces which can have two different terminations, the average of the Ni and Al terminations is given in Table VI. It is this average that is involved in cleavage energy calculations. Table VI shows that both potentials tend to underestimate surface energies, which is a well-known trend of EAM-type potentials. Note that surface energies were not included in the potential fits.

Both the LG and our potentials reproduce the effect of rippled relaxation of the (110) surface that has been established both experimentally[88,89] and by *ab initio* calculations[2,10] (Table VII). The stoichiometric near-surface layers split into sublayers in a manner where Al atoms of the topmost layer relax outwards while Ni atoms relax inwards. The second layer is expected to show an opposite effect, i.e., Al atoms relax inwards and Ni atoms outwards, etc. Both potentials are in agreement with this picture, but tend to overestimate the amount of relaxations. With the present potential, the amount of overestimation is slightly smaller.

Generalized stacking faults have been studied using the γ-surface technique.[90,91] A γ surface represents a plot of the partially relaxed fault energy as a function on the shift vector on a chosen crystallographic plane. The partial relaxation only includes atomic displacements normal to the fault plane, while displacements parallel to the fault plane are prohibited. γ surfaces are useful for predicting preferred dislocation slip systems as they contain information about dislocation Burgers vectors, possible dislocation dissociations, and planar faults resulting from such dissociations. Local minima on a γ surface correspond to stable faults, while local maxima represent barriers that need to be overcome for creating stable faults and/or nucleating dislocations.

TABLE VII. Atomic relaxation of the (110) surface of $B2$-NiAl calculated with the present EAM potential and LG potential (Ref. 33) in comparison with experimental data and *ab initio* calculations. The values represent percent changes Δd_{ij}^{α} (α = Ni or Al), in interlayer spacing between layers i and j of Ni or Al atoms relative to the ideal spacing in the perfect lattice. The asterisk indicates that second layer was fixed.

	Δd_{12}^{Ni} (%)	Δd_{12}^{Al} (%)	Δd_{23}^{Ni} (%)	Δd_{23}^{Al} (%)
Experiment				
LEED[a]	−4.6	5.2	1.0	2.0
MEIS[b]	−7.0±2.0	5.0±2.0	1.0±2.0	−1.0±2.0
Ab initio				
FLAPW[c]	−8.0±0.5	1.5±0.5	0.0*	0.0*
MBPP[d]	−6.9	6.6	0.0*	0.0*
PWPP[e]	−7.0	4.5	0.0*	0.0*
Potentials				
LG	−12.6	8.6	6.4	−5.1
EAM	−11.5	4.3	5.1	−3.9

[a]Low-energy electron diffraction (Ref. 88).
[b]Medium-energy ion scattering (Ref. 89).
[c]Full-potential linearized augmented plane-wave method (Ref. 2).
[d]Mixed-basis pseudopotential method (Ref. 2).
[e]Plane-wave pseudopotential method (Ref. 10).

Figure 11 illustrates the calculated sections of γ surfaces on the (110) and (210) planes in the [111] directions. The local minima indicated by arrows represent stable APB's with partially relaxed energies of 0.64 and 0.78 J/m^2, respectively. The fully relaxed APB energies are smaller: 0.55 and 0.72 J/m^2, respectively (Table VI). Although lower than the APB energies calculated with the LG potential, they are high
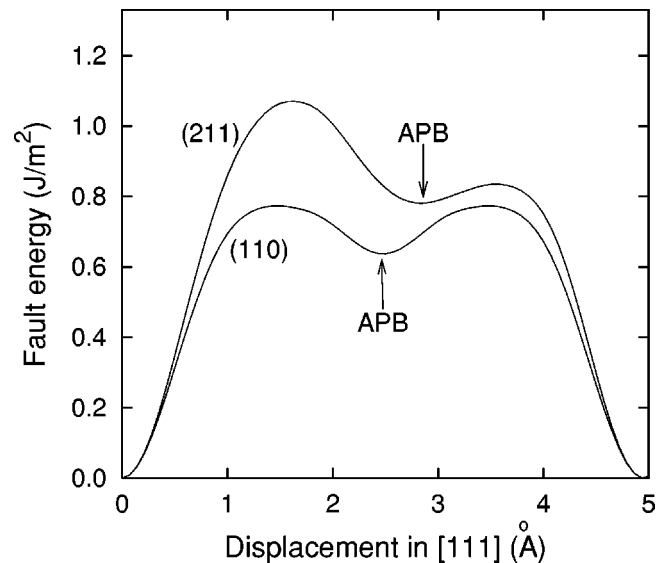

FIG. 11. Calculated sections of the gamma surfaces of $B2$-NiAl on the (110) and (211) planes in the [111] direction. The arrows indicate displacements corresponding to equilibrium antiphase boundaries (APB).

enough to make the dissociation width of $\frac{1}{2}$ [111] partials below the resolution of electron microscopy in agreement with experiments.[47] It is the high APB energies that makes the [111] slip in $B2$-NiAl unfavorable in comparison with the [001] slip observed experimentally.[92] It should be mentioned that atomic relaxations associated with APB's are very significant. Because the potential is fit accurately to LAPW energies of APB-like supercells, the unrelaxed (110) APB energy is close to the respective LAPW value (~ 1.1 J/m^2), but atomic relaxations in a large simulation block reduce this energy by almost 50%.

The unstable fault energies (γ_{us}) corresponding to [001] slip on the (110) and (100) planes have also been calculated to give 0.83 and 1.24 J/m^2, respectively. Both values are close to those obtained with the LG potential, but are significantly lower than the respective *ab initio* values.[12,13] It should be remembered, however, that the mechanical behavior of a material depends more on the ratio $\gamma/\gamma_{\mathrm{us}}$, where γ is the relevant surface energy, rather than on γ_{us} and γ individually.[93] According to Rice,[93] for a bcc material to be ductile the ratio $\gamma/\gamma_{\mathrm{us}}$ must be larger than 5. Using the above values of γ_{us} and the surface energies listed in Table VI, the potential gives $\gamma/\gamma_{\mathrm{us}} = 1.35$ and 1.51 for the [001](110) and [001](100) slip systems, respectively. Both values are well below Rice's threshold value, which is consistent with the experimentally observed intrinsic brittleness on $B2$-NiAl.[92] Thus, even though the absolute values of γ_{us} and γ are below the respective *ab initio* values, the basic mechanical behavior $B2$-NiAl is represented by the potential correctly.

D. Point defects

Thermodynamic and physical properties of strongly ordered compounds near the stoichiometry are strongly influenced by point defects. In some $B2$-ordered intermetallics, particularly $B2$-NiAl, the role of point defects is even more significant and intriguing in view of the different mechanisms of atomic disorder on either side of the stoichiometry. Experimental lattice parameter measurements[53,54] and recent *ab initio* calculations[7,18,19,21,51] both suggest that the off-stoichiometry of Al-rich compositions of $B2$-NiAl is maintained by structural vacancies on the Ni sublattice (triple-defect mechanism: see Sec. I). On the other hand, more recent x-ray measurements reveal some deviations from this mechanism at high temperatures, including lower concentrations of Ni vacancies (V_{Ni}) and higher concentrations of Al$_{\mathrm{Ni}}$ antisites (Al atom on the Ni sublattice), than is predicted by the triple-defect model.[55] Even though these results have been questioned[58] and do not allow us to refute the existance of structural vacancies at low temperatures, this controversy indicates that the domain of validity of the triple-defect model for $B2$-NiAl is not quite certain[56,57] and further investigations are essential for clarifying the issue.

Table VIII summarizes the so-called "raw" formation energies ε_P, entropies s_P, and volumes Ω_P ($P = V_{\mathrm{Ni}}$, V_{Al}, Al$_{\mathrm{Ni}}$, and Ni$_{\mathrm{Al}}$) of point defects in $B2$-NiAl calculated with the present potential. The calculations have been performed using an $8 \times 8 \times 8$ (1024-atom) simulation block with periodic boundary conditions. Upon creating a defect, the total

TABLE VIII. "Raw" formation energies (ε_P), entropies (s_P), and volumes (Ω_P) of individual point defects in $B2$-NiAl calculated with the present EAM potential. Equilibrium point-defect concentrations can be calculated from these data using the cohesive energy $E_0 = -4.465$ eV/atom, entropy $s_0 = 6.311 k_B$/atom, and volume $\Omega_0 = 11.681$ Å^3/atom of the perfect lattice.

Defect	ε_P (eV)	s_P/k_B	Ω_P/Ω_0
V_{Ni}	5.681	-6.935	-0.156
V_{Al}	5.646	-2.721	-0.239
Al$_{\mathrm{Ni}}$	2.915	0.066	0.799
Ni$_{\mathrm{Al}}$	-0.151	4.837	-0.031

energy of the block is minimized with respect to both local atomic displacements and volume relaxation. The defect entropy is associated with atomic vibrations and is included in the classic quasiharmonic approximation.[86,94] The "raw" energy (entropy, volume) of a defect equals the energy (entropy, volume) of the relaxed block containing a single defect minus the energy (entropy, volume) of the initial perfect-lattice block. Thus the "raw" quantities do not include any corrections for the change in the block composition due to the introduction of the defect.

Although the "raw" quantities relating to an individual defect are not sufficient for a full evaluation of its properties, the whole set of "raw" quantities for all four types of point defects, together with the relevant perfect-lattice characteristics, forms a complete data set for calculating the equilibrium defect concentrations. Such calculations are based on a model describing "chemical" equilibrium in a four-component lattice gas of noninteracting point defects.[18,36,95] The data listed in Table VIII are fed into the model in the form of "raw" free energies g_P of individual defects, calculated by[36,95]

$$g_P = \varepsilon_P - T_{s_P} + p\Omega_P, \qquad (16)$$

p being the external pressure and T the temperature. The input set also includes the cohesive energy $E_0 = -4.465$ eV/atom, entropy $s_0 = 6.311 k_B$/atom, and volume $\Omega_0 = 11.681$ Å^3/atom of the defect-free lattice.[98]

Figure 12 presents the equilibrium point-defect concentrations calculated from the model at $T = 1000$ K and $p = 0$ in two ways. In Fig. 12(a), the calculation properly includes the defect entropies s_P through Eq. (16), while in Fig. 12(b) such entropies are intentionally discarded. In the latter case, the temperature enters the model only through the configurational entropy of the defect subsystem. It should be emphasized that all previous calculations have been performed in this approximation. In both cases, Al-rich compositions are strongly dominated by Ni vacancies in agreement with the triple-defect model. The predominance of Ni vacancies also pertains at higher temperatures. The effect of the defect entropies is manifested in some increase in the concentrations of thermal defects, in particular vacancies in Ni-rich compositions and Al$_{\mathrm{Ni}}$ antisites in Al-rich compositions. However,
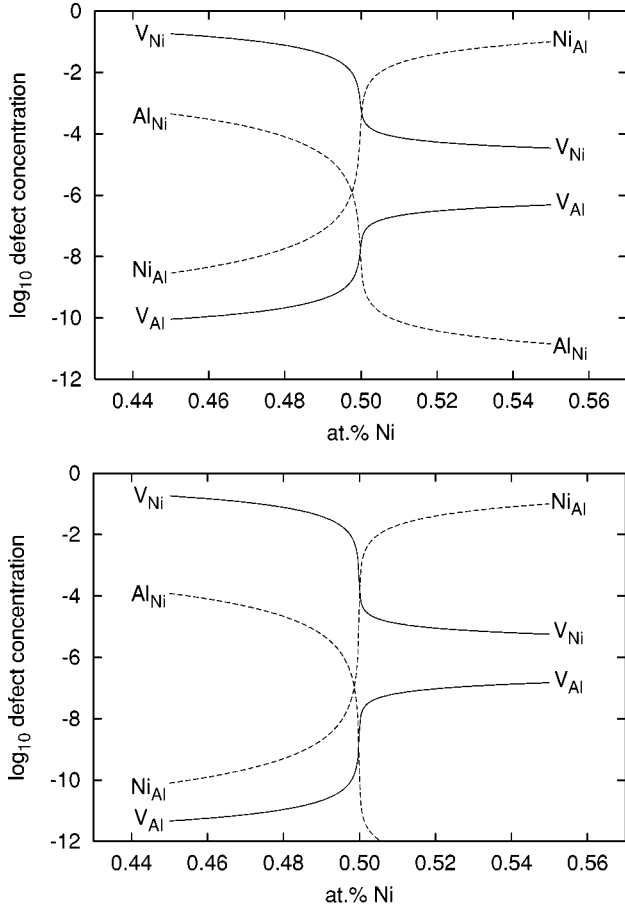
FIG. 12. Calculated equilibrium concentrations (per sublattice site) of vacancies (solid lines) and antisites (dashed lines) in $B2$-NiAl as functions of composition at 1000 K. (a) Calculation including point-defect entropies. (b) Calculation neglecting point-defect entropies ($s_P = 0$).

such concentrations remain much lower than those reported in the experiments of Kogachi *et al.*[55]

Another way of assessing the disorder mechanism is by examining free energies of composition-conserving defect complexes, such as the double vacancy ($V_{Ni} + V_{Al}$), the exchange defect ($Ni_{Al} + Al_{Ni}$), and the triple defects on the Ni sublattice ($2V_{Ni} + Ni_{Al}$) and the Al sublattice ($2V_{Al} + Al_{Ni}$).[19,36,95] The defects involved in such complexes are considered to be separated well enough so that we can neglect their interaction. It can be shown that for Ni structural vacancies to be more favorable in Al-rich compositions than Al_{Ni} antisites, the free energy of the exchange defect should be significantly higher than the free energy of the triple Ni defect. Likewise, for Ni_{Al} antisites to be more favorable in Ni-rich compositions than Al vacancies, the free energy of the triple Al defect should be significantly higher than the free energy of the exchange defect. The respective free-energy differences (or simply energy differences at $T = 0$) are called interbranch-Al and interbranch-Ni energies[19] or stability factors.[34] For $B2$-NiAl to be a triple-defect compound, both interbranch energies should be large enough and positive.

Table IX presents the energies and entropies of the composition-conserving complexes calculated with the present and LG potentials. The second column details the expressions for the complex energies in terms of "raw" energies of individual defects.[18,19,36,95] Similar expressions hold for the complex entropies. The complex energies calculated with the potentials compare well with the *ab initio* energies within the large scatter of such energies. However, while the interbranch-Al energy predicted by the present potential is reasonably high and lies within the range of *ab initio* values, the LG potential predicts a significantly smaller value, which is close to the thermal energy $k_B T$ at 1000 K.

TABLE IX. Energies (in eV) and entropies (normalized to k_B) of composition-conserving point-defect complexes in $B2$-NiAl calculated with the present EAM potential and LG potential (Ref. 33). *Ab initio* energies calculated previously are included for comparison.

Complex	Equation	*Ab initio* Energy	EAM		LG	
			Energy	Entropy	Energy	Entropy
Exchange	$\varepsilon_{Ni_{Al}} + \varepsilon_{Al_{Ni}}$	3.15,[a] 3.10[b] 3.36,[c] 2.65[d]	2.765	4.903	2.788	4.170
Divacancy	$\varepsilon_{V_{Ni}} + \varepsilon_{V_{Al}} + 2E_0$	3.07,[a] 2.71[b] 2.53,[c] 2.18[d]	2.396	2.965	2.630	2.694
Triple-Ni	$2\varepsilon_{V_{Ni}} + \varepsilon_{Ni_{Al}} + 2E_0$	2.83,[a] 2.22[b] 2.36,[c] 1.58[d]	2.281	3.588	2.708	4.199
Triple-Al	$2\varepsilon_{V_{Al}} + \varepsilon_{Al_{Ni}} + 2E_0$	6.46,[a] 6.30[b] 6.32,[c] 5.44[d]	5.276	7.245	5.341	5.359
Interbranch-Ni	$2\varepsilon_{V_{Al}} - \varepsilon_{Ni_{Al}} + 2E_0$	3.31,[a] 3.20[b] 2.69,[c] 2.78[d]	2.511	2.341	2.553	1.190
Interbranch-Al	$\varepsilon_{Al_{Ni}} - 2\varepsilon_{V_{Ni}} - 2E_0$	0.32,[a] 0.88[b] 1.28,[c] 1.07[d]	0.484	1.315	0.079	−0.029

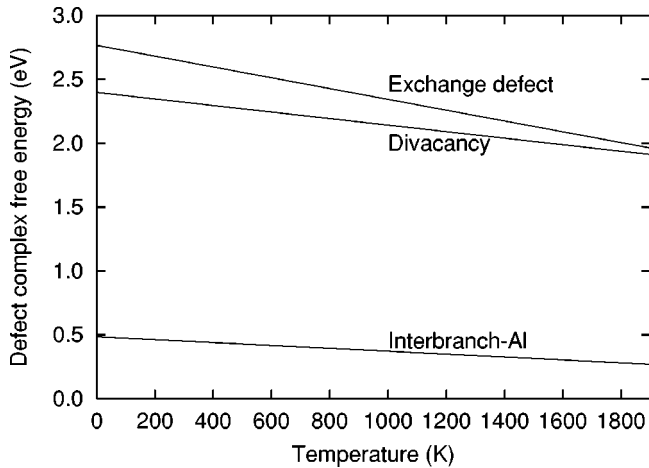[a]Reference 7.
[b]Reference 18.
[c]Reference 19.
[d]Reference 21.

FIG. 13. Calculated free energies of divacancies, exchange defects, and interbrach-Al in $B2$-NiAl as functions of temperature.

In Fig. 13, some of the complex free energies are plotted as functions of temperature. It is observed that the interbranch-Al free energy decreases with temperature, indicating that the thermodynamic stability of Ni structural vacancies relative to Al_{Ni} antisites tends to decline at high temperatures. However, this free energy remains high and positive (0.267 eV) even at the temperature of 1911 K corresponding to the experimental melting point of $B2$-NiAl. The divacancy and exchange defect free energies also decrease with temperature, suggesting that high temperatures favor the formation of additional vacancies and antisites. These trends are in good agreement with direct calculations of point-defect concentrations at high temperatures (see, for example, Fig. 12).

The LG potential shows qualitatively similar trends as in Fig. 13 for divacancies and exchange defects, but the interbranch-Al free energy remains at the same low level (about 0.08 eV) almost independently of the temperature. For Al-rich compositions, the potential still predicts more Ni vacancies than Al_{Ni} antisites, but the difference in the respective concentrations is about an order of magnitude, which is much smaller than with our potential.

IV. SUMMARY

The potential proposed in this work has been constructed using experimental data and a large set of *ab initio* (LAPW) structural energies. Previous work shows that *ab initio* input improves the accuracy and global reliability of semiempirical potentials.[41,44,99,100] Such improvements are due to the fact that *ab initio* data increase the size of the fitting database and, perhaps more importantly, sample a larger area of configuration space than can be sampled by experimental properties alone.

In contrast to other potentials for NiAl, the present one does not reuse any previously generated pure Ni or pure Al potentials. Instead, all seven potential functions involved in the problem have been optimized simultaneously to provide the best fit to $B2$-NiAl properties and give reasonable results for other phases of the Ni-Al system. By construction,

this potential is intended for atomistic simulations of $B2$-NiAl. It does not guarantee accurate results when used for other phases of the system. Such phases have only been included in the potential generation procedure in order to improve its transferability to various local atomic configurations that can be encountered in atomic simulations of $B2$-NiAl. If, for example, pure Ni or Al is to be simulated, other potentials available in the literature will give more accurate results.[41,44,79] This approach is justified physically, because there is no reasons to believe that Ni-Ni or Al-Al interactions in a Ni-Al compound should be exactly the same as in pure Ni or Al. At the same time, the simultaneous optimization of all seven potential functions was the only way we could achieve a satisfactory fit to the large number of target values available for $B2$-NiAl. It should be emphasized, however, that even with 30 adjustable parameters available to us, the fitting database is still underdetermined. Even though the large size of the database could warrant more fitting parameters, we preferred to keep the potential functions simple and avoid possible bumps, wiggles, and other features that inevitably appear on the functions when the number of fitting parameters becomes too large. In other words, we chose to trade some accuracy of the fit for the use of "well-behaved" potential functions and thus more confidence that the potential will not give any surprises in its applications.

The potential provides an accurate fit to basic lattice properties of $B2$-NiAl, including also thermal expansion, which is of importance for high-temperature atomistic simulations using molecular dynamics and Monte Carlo methods. The potential correctly reproduces planar fault characteristics, in particular giving 0.55 J/m^2 for the (110) APB energy in agreement with experimental data.[47] All other stable fault energies and the ratios of unstable fault energies to surface energies are also consistent with the experimentally observed mechanical behavior of $B2$-NiAl. For point defects, a reasonable value of 0.48 eV is obtained for the interbranch-Al energy at zero temperature. This value compares well with previous *ab initio* calculations and, in combination with other point-defect energies, correctly predicts $B2$-NiAl to be a triple-defect compound,[53,54] dominated by Ni structural vacancies in Al-rich compositions and Ni antisites in Ni-rich compositions. Furthermore, calculations with this potential show that point-defect entropies have a noticeable effect on the defect concentrations at high temperatures. Such entropies tend to increase the concentrations of thermal vacancies and antisites in comparison with calculations where point-defect entropies are neglected. This trend may have important consequences for the diffusion behavior of the compound. Despite this trend, however, the off-stoichiometry of the compound is accommodated predominantly by Ni antisites in Ni-rich compositions and Ni vacancies in Al-rich compositions up to the melting point. Thus, even at high temperatures, our calculations do not confirm the significant deviations from the triple-defect model suggested by Kogachi *et al.* based on their high-temperature x-ray measurements or the idea that $B2$-NiAl is intrinsically an antisite disorder compound and not a triple-defect one.[56,57]

ACKNOWLEDGMENTS

[1] *Intermetallic Compounds: Structural Applications*, edited by J. H. Westbrook and R. L. Fleischer (Wiley, New York, 2000), Vol. 4.

[2] J. I. Lee, C. L. Fu, and A. J. Freeman, Phys. Rev. B **36**, 9318 (1987).

[3] T. Hong and A. J. Freeman, Phys. Rev. B **43**, 6446 (1991).

[4] M. H. Yoo and C. L. Fu, Scr. Metall. Mater. **25**, 2345 (1991).

[5] Z. M. Lu, S. H. Wei, and A. Zunger, Acta Metall. Mater. **40**, 2155 (1992).

[6] C. L. Fuand M. H. Yoo, Acta Metall. Mater. **40**, 703 (1992).

[7] C. L. Fu, Y. Y. Ye, M. H. Yoo, and K. M. Ho, Phys. Rev. B **48**, 6712 (1993).

[8] M. J. Mehl, D. J. Singh, and D. A. Papaconstantopoulos, Mater. Sci. Eng., A **170**, 49 (1993).

[9] M. J. Mehl, B. M. Klein, and D. A. Papaconstantopoulos, *Intermetallic Compounds* (Wiley, New York, 1994), Vol. 1, Chap. 9, p. 195.

[10] A. T. Hanbicki, A. P. Baddorf, E. W. Plummer, B. Hammer, and M. Scheffler, Surf. Sci. **331−333**, 811 (1995).

[11] D. G. Pettifor, M. Aoki, P. Gumbsch, A. P. Horsfield, D. N. Manh, and V. Vitek, Mater. Sci. Eng., A **192**, 24 (1995).

[12] R. Wu, L. P. Zhong, L. J. Chen, and A. J. Freeman, Phys. Rev. B **54**, 7084 (1996).

[13] N. I. Medvedeva, O. N. Mryasov, Y. N. Gornostyrev, D. L. Novikov, and A. J. Freeman, Phys. Rev. B **54**, 13 506 (1996).

[14] J. Mei, B. R. Cooper, and S. P. Lim, Phys. Rev. B **54**, 178 (1996).

[15] O. Y. Kontsevoi, O. N. Mryasov, Y. N. Gornostyrev, A. J. Freeman, M. I. Katsnelson, and A. V. Trefilov, Philos. Mag. Lett. **78**, 427 (1998).

[16] M. Šob, L. G. Wang, and V. Vitek, Philos. Mag. B **78**, 653 (1998).

[17] V. Paidar, L. G. Wang, M. Šob, and V. Vitek, Modell. Simul. Mater. Sci. Eng. **7**, 369 (1999).

[18] B. Meyer and M. Fähnle, Phys. Rev. B **59**, 6072 (1999).

[19] P. A. Korzhavyi, A. V. Ruban, A. Y. Lozovoi, Y. K. Vekilov, I. A. Abrikosov, and B. Johansson, Phys. Rev. B **61**, 6003 (2000).

[20] A. Y. Lozovoi, A. Alavi, and M. W. Finnis, Phys. Rev. Lett. **85**, 610 (2000).

[21] A. Y. Lozovoi, A. Alavi, P. A. Korzhavyi, and M. W. Finnis, in *Properties of Complex Inorganic Solids*, edited by A. Meike, A. Gonis, P. E. A. Turchi, and K. Rajan (Plenum, New York, 2000), Vol. 2, p. 439.

[22] N. Bornsen, G. Bester, B. Meyer, and M. Fähnle, J. Alloys Compd. **308**, 1 (2000).

[23] M. S. Daw and M. I. Baskes, Phys. Rev. B **29**, 6443 (1984).

[24] M. W. Finnis and J. E. Sinclair, Philos. Mag. A **50**, 45 (1984).

[25] R. Schroll, V. Vitek, and P. Gumbsch, Acta Mater. **46**, 903 (1998).

[26] R. Schroll, M. W. Finnis, and P. Gumbsch, Acta Mater. **46**, 919 (1998).

[27] P. Gumbsch and R. Schroll, Intermetallics **7**, 447 (1999).

[28] M. Yan, V. Vitek, and S. P. Chen, Acta Mater. **44**, 4351 (1996).

[29] Y. Mishin and D. Farkas, Philos. Mag. A **78**, 29 (1998).

[30] D. Farkas, J. Phys.: Condens. Matter **12**, R497 (2000).

[31] M. Ludwig and P. Gumbsch, Acta Mater. **46**, 3135 (1998).

[32] D. Farkas, Philos. Mag. A **80**, 1425 (2000).

[33] M. Ludwig and P. Gumbsch, Modell. Simul. Mater. Sci. Eng. **3**, 201 (1995).

[34] Y. Mishin and D. Farkas, Philos. Mag. A **75**, 169 (1997).

[35] Y. Mishin and D. Farkas, Philos. Mag. A **75**, 187 (1997).

[36] M. Hagen and M. W. Finnis, Philos. Mag. A **77**, 447 (1998).

[37] S. Divinski and Chr. Herzig, Intermetallics **8**, 1357 (2000).

[38] S. Frank, S. V. Divinski, U. Södervall, and Chr. Herzig, Acta Mater. **49**, 1399 (2001).

[39] M. Yan, M. Šob, D. E. Luzzi, V. Vitek, G. J. Ackland, M. Methfessel, and C. O. Rodriguez, Phys. Rev. B **47**, 5571 (1993).

[40] D. T. Kulp, G. J. Ackland, M. Šob, V. Vitek, and T. Egami, Modell. Simul. Mater. Sci. Eng. **1**, 315 (1993).

[41] F. Ercolessi and J. B. Adams, Europhys. Lett. **26**, 583 (1994).

[42] A. Landa, A. Ruban, P. Wynblatt, H. Skriver, A. Girshick, and V. Vitek, J. Phys.: Condens. Matter **10**, 5717 (1998).

[43] A. Landa, P. Wynblatt, A. Girshick, V. Vitek, A. Ruban, and H. Skriver, Acta Mater. **46**, 3027 (1998).

[44] Y. Mishin, D. Farkas, M. J. Mehl, and D. A. Papaconstantopoulos, Phys. Rev. B **59**, 3393 (1999).

[45] Y. Mishin, M. J. Mehl, D. A. Papaconstantopoulos, A. F. Voter, and J. D. Kress, Phys. Rev. B **63**, 224106 (2001).

[46] M. I. Baskes, Acta Metall. Sin. **8**, 287 (1995).

[47] P. Veyssiére and R. Noebe, Philos. Mag. A **65**, 1 (1992).

[48] S. Rubini and P. Ballone, Phys. Rev. B **48**, 99 (1993).

[49] D. Farkas, B. Mutasa, C. Vailhe, and K. Ternes, Modell. Simul. Mater. Sci. Eng. **3**, 201 (1995).

[50] S. I. Rao, C. Woodward, and T. A. Parthasarathy, in *High Temperature Ordered Intermetallic Alloys IV*, edited by L. Johnson, D. P. Pope, and O. Stiegler, Mater. Res. Soc. Symp. Proc. No. 213 (Materials Research Society, Pittsburgh, 1991).

[51] A. Alavi, A. Y. Lozovoi, and M. W. Finnis, Phys. Rev. Lett. **83**, 979 (1999).

[52] We use the predominance of vacancies and antisites on different sides of the stoichiometry at a given temperature as a working definition of a triple-defect compound, which is sufficient for the purposes of this paper. There are other, more rigorous definitions in terms of ground-state energies of composition-conserving defect complexes; see, for example, Ref. 19.

[53] A. J. Bradley and A. Taylor, Proc. R. Soc. London, Ser. A **159**, 56 (1937).

[54] A. Taylor and N. J. Doyle, J. Appl. Crystallogr. **5**, 201 (1972).

[55] M. Kogachi, T. Tanahashi, Y. Shirai, and M. Yamaguchi, Scr. Metall. Mater. **34**, 243 (1996).

[56] X. Ren, K. Otsuka, and M. Kogachi, Scr. Mater. **41**, 907 (1999).

[57] X. Ren and K. Otsuka, Philos. Mag. A **80**, 467 (2000).

[58] B. Meyer, G. Bester, and M. Fahnle, Scr. Mater. **44**, 2485 (2001).

[59] C. Kittel, *Introduction to Solid State Physics* (Wiley-Interscience, New York, 1986).

[60] R. Hultgren, P. D. Desai, D. T. Hawkins, M. Gleiser, and K. K. Kelley, *Selected Values of the Thermodynamic Properties of Binary Alloys* (ASM, Metals Park, OH, 1973).

[61] N. Rusović and H. Warlimont, Phys. Status Solidi A **44**, 609 (1977).

[62] *Thermal Expansion: Metallic Elements and Alloys*, edited by Y. S. Touloukian, R. K. Kirby, R. E. Taylor, and P. D. Desai, Vol. 12 of *Thermophysical Properties of Matter* (Plenum, New York, 1975).

[63] F. X. Kayser and S. Stassis, Phys. Status Solidi A **64**, 335 (1981).

[64] *Handbook of Chemistry and Physics*, edited by R. C. Weast (CRC, Boca Raton, FL, 1984).

[65] A detailed description of all crystalline structures involved in this work can be found at http://cst-www.nrl.navy.mil/lattice/.

[66] O. K. Andersen, Phys. Rev. B **12**, 3060 (1975).

[67] S. H. Wei and H. Krakauer, Phys. Rev. Lett. **55**, 1200 (1985).

[68] J. P. Perdew and Y. Wang, Phys. Rev. B **45**, 13 244 (1992).

[69] W. Kohn and L. J. Sham, Phys. Rev. **140**, A1133 (1965).

[70] H. J. Monkhorst and J. D. Pack, Phys. Rev. B **13**, 5188 (1976).

[71] M. J. Mehl, J. E. Osburn, and D. A. Papaconstantopoulos, Phys. Rev. B **41**, 10 311 (1990).

[72] M. J. Gillan, J. Phys.: Condens. Matter **1**, 689 (1989).

[73] F. Mattheiss, J. H. Wood, and A. C. Switendick, Methods Comput. Phys. **8**, 63 (1968).

[74] B. N. Harmon, D. D. Koelling, and A. J. Freeman, J. Phys. C **6**, 2294 (1973).

[75] M. J. Mehl, Phys. Rev. B **61**, 1654 (2000).

[76] R. A. Johnson, Phys. Rev. B **39**, 12 554 (1989).

[77] A. F. Voter, *Intermetallic Compounds* (Wiley, New York, 1994), Vol. 1, Chap. 4, p. 77.

[78] For an elemental crystal the curvature of $F(\bar{\rho})$ is proportional to the Cauchy pressure $c_{12} - c_{44}$ and should normally be positive, meaning that $F(\bar{\rho})$ should be a minimum at $\bar{\rho}^0$ in the effective pair format (Ref. 77). In a binary compound, the Cauchy pressure is proportional to a linear combination of the curvatures of the embedding functions $F_A(\bar{\rho})$ and $F_B(\bar{\rho})$, so it is not prohibited for one of them to be a maximum in the effective pair format provided the other one is a minimum.

[79] A. F. Voter and S. P. Chen, in *High Temperature Ordered Intermetallic Alloys II*, edited by N. S. Stoloff, C. C. Koch, C. T. Liu, O. Izmmi, Mater. Res. Soc. Symp. Proc. No. 81 (Materials Research Society, Pittsburgh, 1987).

[80] S. M. Foiles, M. I. Baskes, and M. S. Daw, Phys. Rev. B **33**, 7983 (1986).

[81] Y. Mishin, D. Farkas, M. J. Mehl, and D. A. Papaconstantopoulos, in *Multiscale Modelling of Materials*, edited by T. Diaz de la Rubia, V. Bulatov, N. M. Ghoniem, R. Phillips, E. Kaxiras, and N. Ghoniem, Mater. Res. Soc. Symp. Proc. No. 538 (Materials Research Society, Warrendale, PA, 1999), p. 535.

[82] The potential functions are available for retrieval by FTP over the WWW from ftp://cst-www.nrl.navy.mil/bind/eam/nial.html

[83] M. Mostoller, R. M. Nicklow, D. M. Zehner, S. C. Lui, J. M. Mundenar, and E. W. Plummer, Phys. Rev. B **40**, 2856 (1989).

[84] J. H. Rose, J. R. Smith, F. Guinea, and J. Ferrante, Phys. Rev. B **29**, 2963 (1984).

[85] J. W. Otto, J. K. Vassiliou, and G. Frommeyer, J. Mater. Res. **12**, 3106 (1997).

[86] S. M. Foiles, Phys. Rev. B **49**, 14 930 (1994).

[87] E. C. Bain, Trans. AIME **70**, 25 (1924).

[88] J. R. Noonan and H. L. Davis, Science **234**, 310 (1986).

[89] S. M. Yalisove and W. R. Graham, Surf. Sci. **183**, 556 (1987).

[90] V. Vitek, Philos. Mag. **73**, 773 (1968).

[91] V. Vitek, Cryst. Lattice Defects **5**, 1 (1974).

[92] D. B. Miracle, Acta Metall. Mater. **41**, 649 (1993).

[93] J. R. Rice, J. Mech. Phys. Solids **40**, 239 (1992).

[94] Y. Mishin, M. R. Sørensen, and A. F. Voter, Philos. Mag. A **81**, 2591 (2001).

[95] Y. Mishin and C. Herzig, Acta Mater. **48**, 589 (2000).

[96] M. Ellner, S. Kek, and B. Predel, J. Less-Common Met. **154**, 207 (1989).

[97] *Smithells Metals Reference Book*, 6th ed., edited by E. A. Brandes (Butterworths, London, 1983).

[98] The classical expression for the vibrational entropy contains a factor $k_B T$. The point-defect entropies listed in Table VIII, as well as the perfect-lattice entropy s_0, have been calculated for the reference temperature $T = 1000$ K. The choice of reference temperature does not affect the equilibrium defect concentrations because the $k_B T$ factor cancels out in all expressions that determine such concentrations; see Refs. 94 and 95 for details. The entropies of composition-conserving defect complexes listed in Table IX do not depend on the reference temperature either.

[99] J. N. Murrell, Philos. Mag. A **73**, 163 (1996).

[100] M. I. Baskes, M. Asta, and S. G. Srinivasan, Philos. Mag. A **81**, 991 (2001).